

Membrane Deformation at Integrin Adhesions

Erdinç Atilgan and Ben Ovrin*

Gruss-Lipper Biophotonics Center, Department of Anatomy and Structural Biology, Albert Einstein College of Medicine, Bronx, NY, USA

Abstract: In order to measure the nucleation of new adhesions on the ventral surface of a cell, we have combined phase shifting laser feedback interferometry with a high numerical aperture inverted fluorescence microscope. We use fluorescence to image molecules at the adhesion site and stage scanning interference microscopy in order to measure the distance between the ventral surface of a cell and the substratum with several nanometer precision. Our analytic and Monte Carlo simulations of integrin mediated adhesions predict several features of these new adhesions. An analysis of the energetics of membrane bending and the effects of a composite system of freely diffusing repellers and receptors and a fixed network of ligands on the extracellular matrix predicts that a small bundle of actin filaments should be able to push the membrane down to the extracellular matrix and nucleate a new adhesion with critical radius below the diffraction limit. We have obtained a map of the reflectivity of the ventral surface of fixed metastatic mammary adenocarcinoma cells and we have shown that the data are correlated with markers for a focal adhesion adaptor protein. We are modeling the interference of the incident electric field with the field reflected from the ventral surface so as to obtain the surface topography at focal adhesions from the optical phase data.

Keywords: Integrin adhesions, nucleation, critical radius, interference microscopy, phase shifting interferometry.

INTRODUCTION

Adhesion to an extracellular matrix, an essential process in mammalian cellular locomotion, requires interaction between adhesion receptors and their ligands. Cell motility requires cycles of adhesion formation at the front of the cell and the disruption of adhesive forces at the tail of the cell [1, 2]. We have recently developed a model that provides a mechanistic understanding of the processes that govern the formation of integrin adhesions *ex novo* from an essentially planar plasma membrane [3]. This model describing the mechanisms that lead to the birth of an adhesion site predicts the characteristics of this earliest adhesion, which we call a new adhesion. The new adhesion is distinguished from more mature adhesions because it is not initially anchored to the cytoskeleton by protein interactions on the cytoplasmic face. Unlike other integrin adhesion sites, such as focal complexes, focal adhesions, fibrillar adhesions and podosomes, we predict that the new adhesion begins as an adhesion patch that has a radius below the diffraction limit of light ($\approx 250\text{nm}$). The characteristics of this early adhesion, however, will change with time and it will either remodel to become a larger focal adhesion or it will vanish [4, 5].

This model stipulates that, although integrin activation is a necessary condition for ligand binding, it is not a sufficient condition because the stalks of the conformationally activated heterodimer have relatively short projections from the plasma membrane into the extracellular space and longer molecules on the crowded membrane surface sterically inhibit the extended integrins from binding to their ligands

[6-11]. Therefore, the ligand binding domain needs to be displaced so that it can reach a ligand on the extracellular matrix (ECM). Our model predicts that polymerizing actin filaments locally deform the membrane and translate integrin's extracellular binding domain toward the ECM (Fig. 1).

We envision the formation of an integrin adhesion as a process that begins with local membrane bending, a redistribution of long molecules from the adhesion site and culminates with integrin aggregation. This is contrary to many published models of integrin adhesions that present schematic pictures of a globally flat membrane that contains transmembrane integrin segments spanning the lipid bilayer [12, 13]. The evidence for local membrane bending is based upon data from Interference Reflection Microscopy and electron microscopy experiments which indicate that membrane deformation is associated with adhesion and that the plasma membrane at an integrin adhesion appears to be closer to the substrate than adjacent regions (a distance of approximately 30nm) [14, 15]. Therefore, these data suggest that activated integrins bind to ligands on the ECM in regions of membrane that have bent toward the substrate. Our model, which is based upon an analysis of the free energy landscape of a system of freely diffusing receptors and repeller molecules and a dynamically deformable membrane, predicts the nucleation, growth, disassembly and merging of new adhesions.

In order to verify our model predictions, it is essential to measure some of the properties of the new adhesion. Because the radius of the adhesion is below the diffraction limit of light and the magnitude of the membrane bending is extremely small, this is a very challenging task. In this paper, we introduce an approach for measuring these new adhesions.

*Address correspondence to this author at the Department of Anatomy and Structural Biology, Albert Einstein College of Medicine, 1300 Morris Park Avenue, Bronx, NY 10461, USA; E-mail: bovrin@aecom.yu.edu

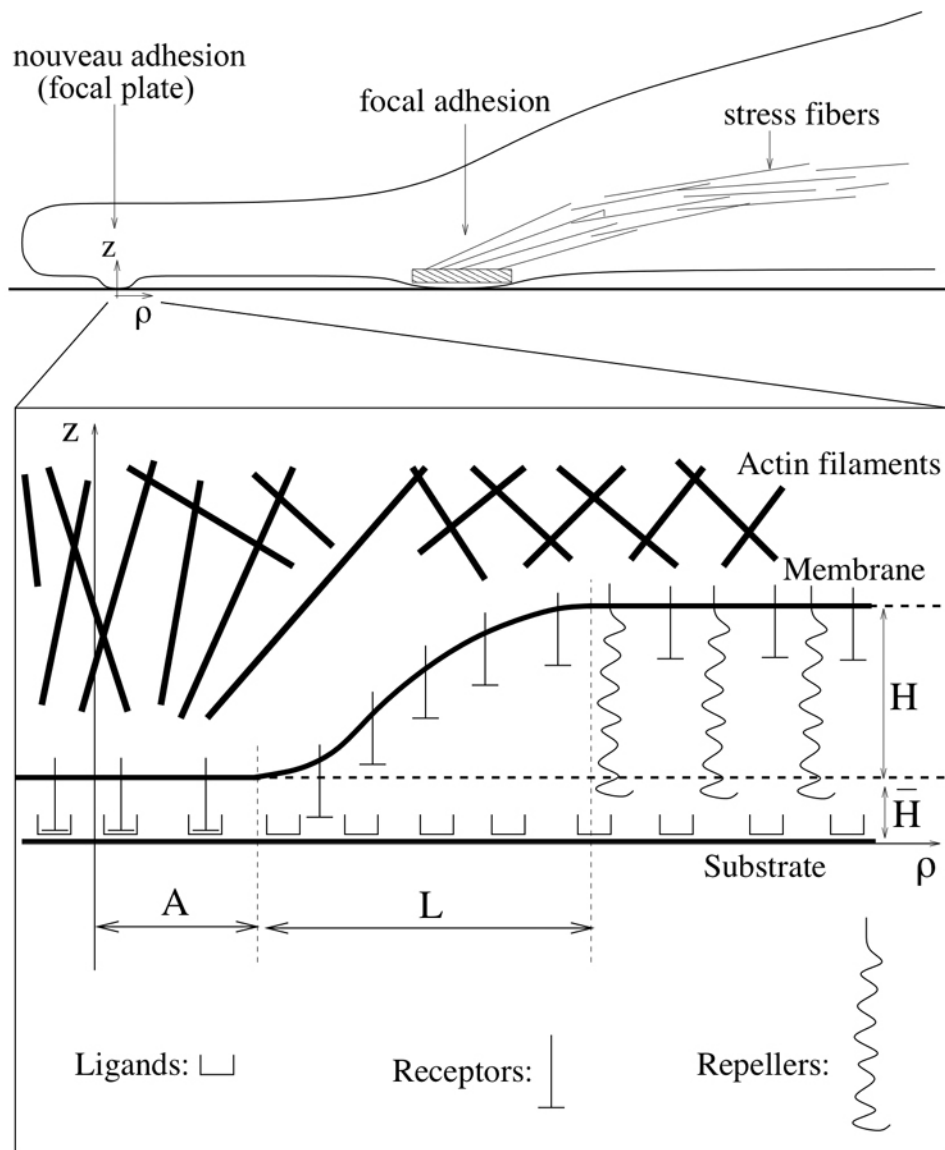


Fig. (1). Model of a nouveau adhesion formed under a planar membrane in the lamellipodium. The membrane is constrained between an actin network on the cytoplasmic face and a layer of freely diffusing repellers which extend toward the substrate. Formation of a nouveau adhesion requires membrane bending and the subsequent exclusion of repeller molecules from the plate region. The membrane profile (solid line) is shown when the repellers are assumed to be rigid molecules.

CHARACTERISTICS OF NOUVEAU ADHESIONS

Our model predicts that the formation of a nouveau adhesion ex novo from an approximately planar membrane requires deformation of the membrane towards the extracellular matrix by $H = 30\text{nm}$ (Fig. 2). An analysis of the energy required to form this nouveau adhesion ex novo predicts that the probability of generating nouveau adhesions solely by thermally induced membrane fluctuations is extremely small. Therefore, the most likely additional energy source which bends the membrane is a coalescence of polymerizing actin filaments; polymerization of actin generates an effective force which depends upon the ratio of the concentration of free actin monomers in the cytoplasm to the critical concentration for polymerization [16].

Although the polymerizing actin network is primarily responsible for the protrusion of the leading edge of the lamellipodium [17], this network is polymerizing in all three dimensions [18] and actin filaments also push the membrane toward the substrate. The majority of polymerizing actin filament tips that reach the membrane on the ventral surface are randomly distributed and maintain the planar membrane shape. It is likely, however, that the coalescence of several filaments may occur and these densely packed regions of actin filament could deform the membrane toward the substrate by an actin ratcheting mechanism that would subsequently establish the first integrin-ligand bonds. Simulations of a three-dimensional actin filament network (see Fig. 9 in [18]) can predict the probability of nucleating an adhesion and the distribution of a coalescence of actin filaments on the ventral surface. Recent experiments have shown that initial

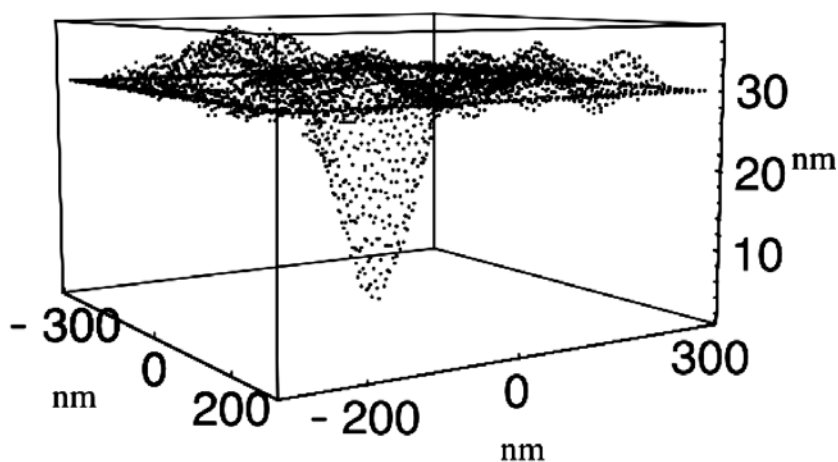


Fig. (2). Results of a Monte Carlo simulation of the membrane shape at a nouveau adhesion. Thermal fluctuations deform the membrane, but are not large enough to push the membrane towards the extracellular matrix such that an adhesion patch may form. Therefore, actin filaments are the most likely mechanism which results in membrane displacement by $H = 30$ nm.

adhesions generally form under the lamellipodium [7, 19] and evidence suggests that the location of the earliest adhesions is correlated with a high concentration of actin barbed ends [20]. These experiments are consistent with our model predictions.

Because the analysis of the energy landscape demonstrates that there is an energy barrier governing the formation of an adhesion from a planar membrane, if a nouveau adhesion forms with an adhesion radius, A (Fig. 1), below the critical radius, A_c , it will not be energetically favorable for the adhesion to grow. Conversely, if a focal plate is formed with a base radius $A > A_c$, then it will be energetically favorable for the plate to continue to form more integrin bonds and the plate will reach a larger radius. The size of the critical radius, which depends upon the density of ligands (integrins) and repeller molecules, is approximately $A_c = 160$ nm. As the nouveau adhesion grows, the number of bound receptors which aggregate on the base increases. The growth rate for this adhesion would be ≈ 30 nm/s. If the nouveau adhesion were to continue to grow at this rate from its critical radius, approximately 100 seconds would be required to reach a radius of $3 \mu\text{m}$ [3].

IMAGING OF NOUVEAU ADHESIONS

Because our model predicts both a low density of nouveau adhesions on the ventral surface of a cell and adhesions with initial radii below the diffraction limit, imaging these early adhesions will not be trivial. Rather than image the entire ventral surface of a cell, however, it is possible to concentrate predominantly on the lamellipodium because this region should have the greatest concentration of nouveau adhesions. The imaging geometry, with a cell on a flat extracellular matrix, is shown in Fig. (3a). In order to observe nouveau adhesions, it will be essential to image an extremely small aggregation of integrins and measure the subsequent membrane bending. Indeed, if the model predictions are correct, approximately 30 sec will be required before the small adhesion grows to approximately $1 \mu\text{m}$. As shown in Fig.

(3b), cells sit on a transparent substrate (glass with index of refraction ≈ 1.51) and the ventral surface is surrounded by media with index of refraction of ≈ 1.34 (buffer) and ≈ 1.36 (cytoplasm). A high numerical aperture (NA) oil objective is employed for all imaging.

In order to measure the topography of the membrane, we are implementing a form of interference microscopy. As shown in Fig. (3b), the incident electric field is both transmitted and reflected at the interface between the glass-buffer interface. After refraction at the glass-buffer interface, part of the transmitted field reflects from the ventral surface of the membrane and is subsequently collected with the objective.

We have implemented a form of interference microscopy, called laser feedback microscopy, that is somewhat analogous to interference reflection microscopy. Interference Reflection Microscopy was introduced over forty years ago in order to measure the adhesion of cells to a substratum [21]. In this method, a series of interference fringes are observed which encode the distance between the ventral surface and the substratum. As the cell makes contact with the substratum, the optical path length between the interfering rays changes as compared with regions where the membrane is not in contact. This technique, also known as reflection interference contrast microscopy [22], has not generally been used to produce quantitative measurement because it is difficult to interpret the data. Ideally, we require a quantitative method that can rapidly resolve the distance between the cell and the substratum at each point over the cell surface.

LASER FEEDBACK INTERFERENCE MICROSCOPY

Unlike interference reflection microscopy, in our laser feedback interference microscope, we have implemented phase-shifting interferometry to determine the phase and fringe visibility; this is an extremely powerful method and most commercial applications of interference microscopy implement some form of phase shifting interferometry [23]. Rather than analyzing the intensity variations in a single in-

terference pattern, phase shifting interferometry is based upon an analysis of a series of interference patterns, each of which was acquired with a different, experimentally controlled, phase shift. Using phase shifting interferometry, it is possible to separately determine the variation in index of refraction (fringe visibility) from the effect of variations in the height of the ventral surface; using phase measuring techniques, it is therefore possible to determine if a bright fringe is the result of contact between the ventral and the substratum or if it results from the presence of highly reflective material in the cytoplasm.

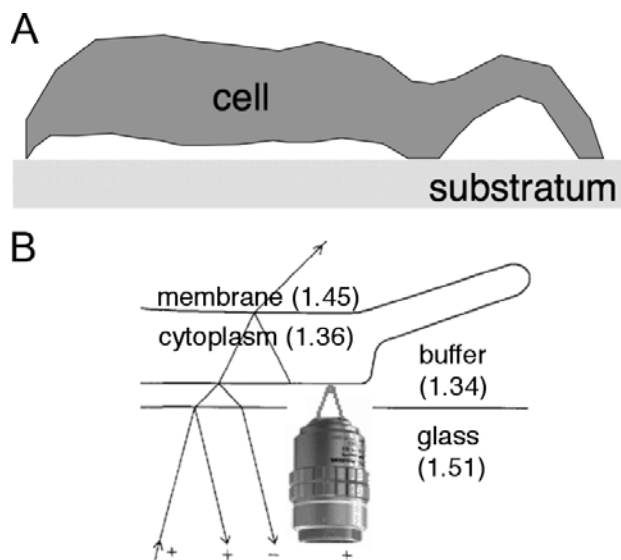


Fig. (3). (A) Schematic diagram of the dorsal and ventral surface of the cell as it rests on the substratum. (B) Imaging geometry and index of refraction for the relevant media.

We have previously coupled a laser feedback interferometer to an optical microscope [24, 25]. In our previous work, we utilized this approach to measure wetting phenomena [26] and we have shown that we can use this method to determine the surface contour and shape of a fluid drop on a silicon surface [27] and that this interference method has the depth sectioning capability of a confocal microscope. This quantitative approach, based upon the application of phase shifting methods to laser feedback interference microscopy, produces two outputs: (1) the visibility of the interference fringes and (2) a phase map that is correlated with the optical path length.

Fig. (4) shows a schematic representation of our laser feedback interferometer coupled to an inverted microscope. Our instrument consists of a helium laser (1107P, Uniphase) that is coupled to the side port of an inverted microscope (TE2000, Nikon). The laser beam propagates through a polarizer, P, an electro-optic modulator, EOM (4002, New Fo-

cus), and is expanded, L_1 , to overfill the back aperture of a high numerical aperture objective (60x/1.4). After reflection from the cell, the laser light re-enters the laser where it interferes with the standing wave in the cavity; this interference changes the intensity of the laser, I_j (Eq. 1), which is monitored with the detector (1201, New Focus) after light propagates through the laser's back mirror. The ventral surface of the cell was scanned using a piezoelectric nanopositioning/scanning stage (Nanobios, Mad City Labs). In addition to the interference arm of the microscope, this inverted microscope is equipped for through-the-objective based total internal reflection and epi-fluorescence.

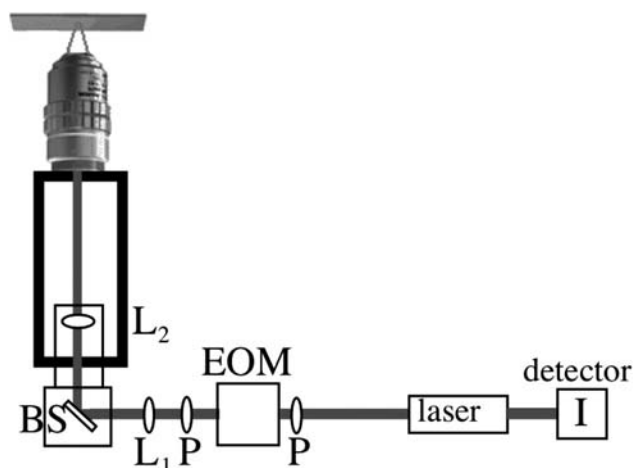


Fig. (4). Schematic of the confocal laser feedback interferometer attached to an inverted microscope. Light from the laser passes through a polarizer, P, an electro-optic modulator, EOM, and another polarizer and an expanding lens L_1 . After reflection from the cell, the light is coupled directly back into the laser cavity. The laser intensity, I , is monitored with the detector. To create an "image" of the cell, the laser beam is held fixed and the cell is scanned using a closed-loop piezoelectric stage.

The laser intensity can be written by Eq. 1:

$$I_j = I_0 \{1 + m \cos (\phi + \Psi_j)\} \quad (1)$$

where I_0 is the overall background (dc) intensity, m is the fringe visibility (also called the contrast) of the interference fringes. The parameter ϕ is related to the product of the index of refraction of the extracellular space and the optical path length from the substratum to the ventral surface (i.e. the path that an optical ray travels). The parameter Ψ_j represents an additional phase shift that is independent of the optical path length and introduced under computer control. The visibility, m , and the phase term, ϕ , provide quantitative information about the reflectivity and the topography of the ventral surface, respectively [24, 25]. To implement phase shifting methods, we apply five discrete voltages to the electro-optic modulator, Ψ_j , and record five intensity values [24]. In order to build up an image, a Labview program addresses the piezoelectric stage via a USB interface. Using custom software, the user provides the number of lines for both the fast and slow scan directions. The user also provides the step size (in nm) for each fast scan pixel. At each pixel, five phase shifts are introduced and both the phase and visibility are

calculated. Currently, 1 second is required to scan 100 pixels with a step size of 100 nm between pixels and on-the-fly display of the both the phase and visibility. This corresponds to a dwell time of 10 msec per pixel. At the end of each fast scan line, the stage is moved by a user defined amount in the orthogonal scan direction and another fast-scan line is acquired. Previously, we have shown that the instrument may be used to quantify dc optical path length changes of less than 1 nm [24, 25]. Currently, with 10 msec per pixel we have a standard deviation of approximately 5 nm.

Calibration of the Interference Microscope

In order to calibrate the instrument, we scanned an optical standard (MRS-4, Geller) using our interference microscope. The standard consists of anti-reflective chromium that consists of a 30nm CrO₂ layer over 70nm of Cr on a transparent quartz substrate. Fig. (5a) shows a reflectivity image from a portion of a 20 μ m x 20 μ m region pattern that consists of 1 μ m lines and 1 μ m spaces. Although this looks like a widefield image, the data were obtained by point-scanning laser feedback interference microscopy. Fig. (5b) shows the sample reflectivity and topography at a line cut at the location of the white bar in Fig. (5a). The data indicates diffraction-limited spatial resolution in the transverse direction.

Imaging Cells with Interference Reflection Microscopy and the Laser Feedback Interference Microscope

We used both Interference Reflection Microscopy and phase-shifted laser feedback interference microscopy to image the ventral surface of motile cells [28]. Non-metastatic, rat mammary cancer (MTC) cells were treated with trypsin and plated on glass bottom dishes (MatTek, Inc.) with no. 1.5 coverslips [29]. The cells were starved for one hour using bovine serum albumin and then stimulated by epidermal growth factor for one minute. Yellow fluorescent protein (YFP) paxillin was transiently transfected into the MTC cells. The cells were then fixed with formaldehyde and kept in tris buffered saline. We imaged the cell using a 100x/1.4 NA objective. Fig. (6a) shows an interference reflection image of a cell fixed on a glass surface. The field diaphragm of the microscope is clearly observed in the image. Using phase shifted laser feedback interference microscopy, we scanned the cell by determining the visibility and phase at each pixel when adjacent pixels were separated by 100nm. In order to compare the data to interference reflection microscopy, we subsequently scaled the data. Fig. (6b) shows the visibility data (m in Eq. 1) and Fig. (6c) shows the optical phase, ϕ , obtained from the ventral surface of the cell. Fig. (6d) shows the distribution of fluorescence from the labeled protein pax-

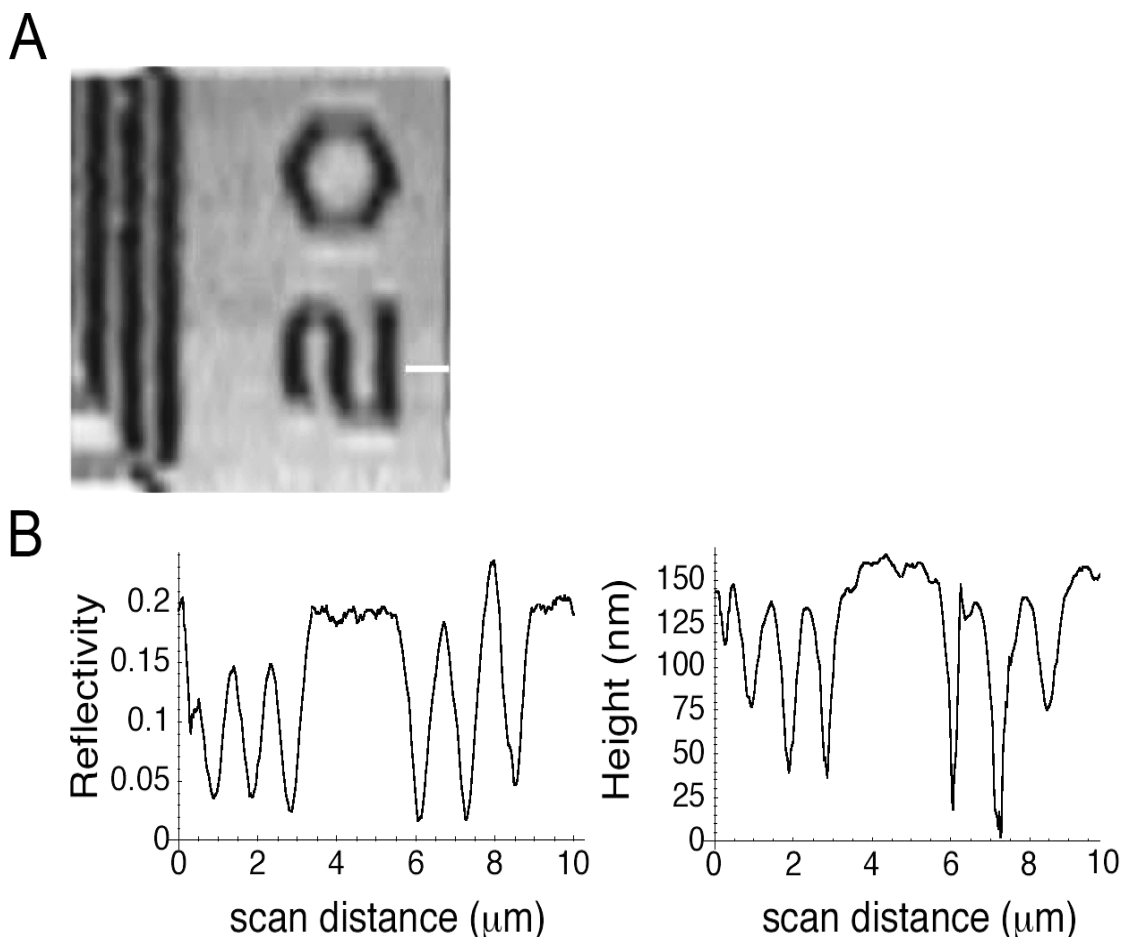


Fig. (5). (A) Reflectivity image of a microscopy reference standard (MRS 4, Geller) obtained with the laser feedback interference microscope. The pattern has a pitch pattern of 1 μ m lines and spaces. (B) Reflectivity and height line cuts, at the location of the bar in (A).

illin along the ventral surface of the cell. Because this protein is known to be concentrated at focal adhesions, this image can be interpreted as a map showing the density and size of focal adhesions along the ventral surface.

DISCUSSION

As a first step towards determining the characteristics of nouveau adhesions, we have applied a laser feedback interference microscope to measure the visibility and phase at

each point on the ventral surface of a fixed cell. We have compared the data with an image that shows the density of paxillin, a protein associated with focal adhesions. The visibility images, obtained with our interference microscope are analogous to the data obtained from the interference reflection microscopy image of the same cell. The paxillin stained regions show as dark spots in both of these images.

In addition to measuring the reflectivity of the ventral surface of the cell, we ultimately need to determine the

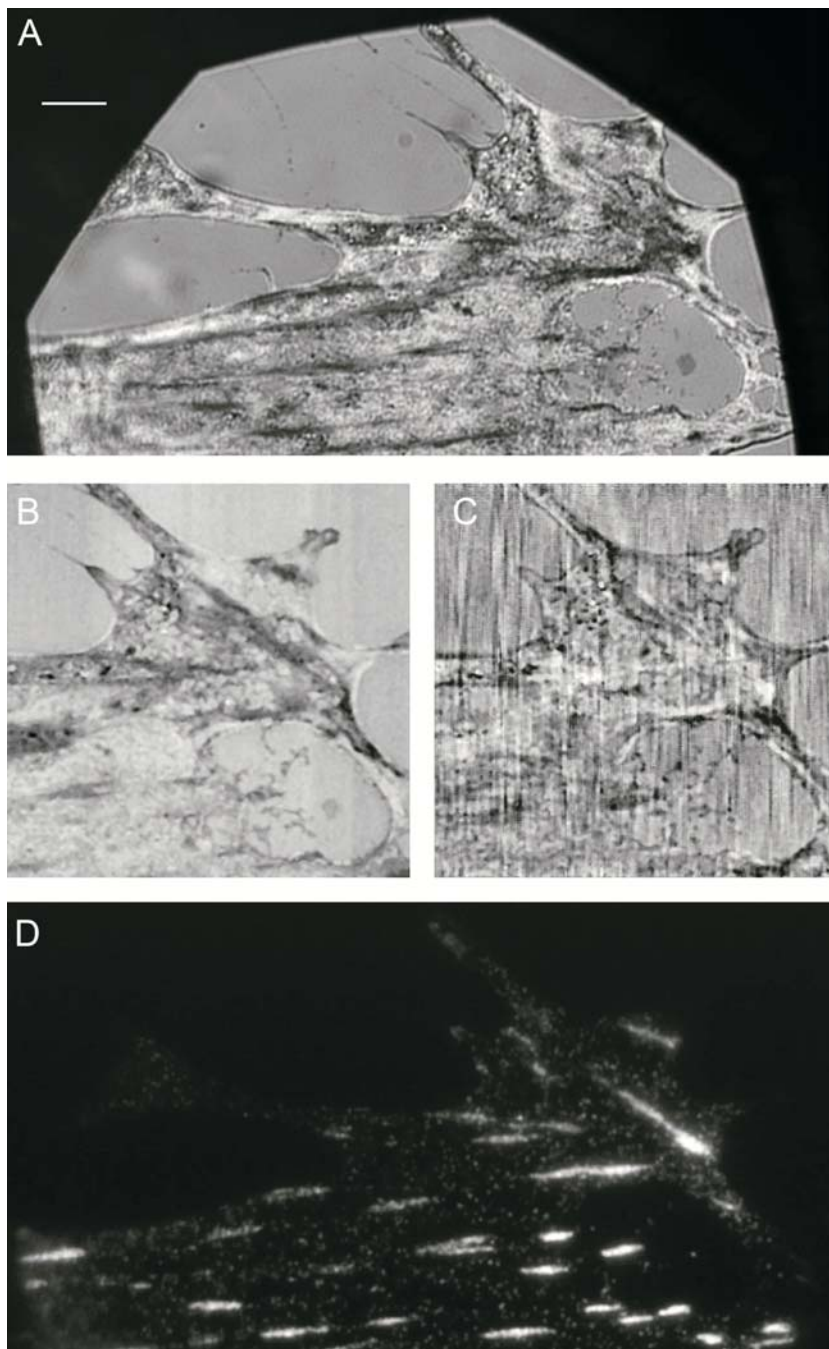


Fig. (6). Data from the ventral surface of a cell on a glass substrate obtained using: **(A)** Interference Reflection Microscopy image (scale bar = 3.2 μm) and **(B & C)** the laser feedback interference microscope. In order to compare the data from the two interference techniques, the reflectivity image **(B)** and phase image **(C)** are scaled to the same size as the interference reflection microscopy **(A)** image. **(D)** Epifluorescence image showing the concentration of paxillin at focal adhesions.

tography of the membrane. Therefore, it is essential to model the interference phase data. Unfortunately, this is not a trivial task. Because the plasma membrane is not a highly reflective material, the data has inherently low signal-to-noise ratio. In addition, the electric field that is collected by the microscope objective may contain a contribution from the ventral surface, internal organelles, actin filaments and the dorsal membrane. Additional complications may arise as a result of polarization changes. We conclude that it is essential to model the distribution and contribution of each of these components.

Because cells are highly complex structures, we are currently imaging controlled, optimized systems including membrane bilayers and spheres. In order to improve the signal-to-noise ratio, we need to average the data. Unfortunately, ambient changes in the environment (e.g. temperature, humidity etc.) lead to large changes in the phase data. Therefore, we plan to decrease the random errors in our measurements by performing experiments in a highly controlled environment.

CONCLUSIONS

Phase shifted laser feedback interference microscopy may potentially be used to obtain information about the reflectivity and membrane topography of the ventral surface of a cell. Although the fringe visibility data may be correlated with the reflectivity at a given pixel, accurate interpretation of the phase data requires a model of the process of fringe formation.

ACKNOWLEDGEMENT

We thank Amber L. Wells for maintaining the cell line. This work was supported by a grant from the National Institutes of Health: R01GM076293 (B.O.).

REFERENCES

- [1] Baily, M. and Condeelis, J. (2002) Cell motility: insights from the backstage. *Nat. Cell Biol.*, **4**, E292-294.
- [2] Lauffenburger, D. and Horwitz, A. (1996) Cell migration: a physically integrated molecular process. *Cell*, **84**, 359-369.
- [3] Atligan, E. and Ovryn, B. (2009) Nucleation and growth of integrin receptors. *Biophys. J.*, **96**, 3555-3572.
- [4] Zaidel-Bar, R.; Milo, R.; Kam, Z. and Geiger, B. (2007) A paxillin tyrosine phosphorylation switch regulates the assembly and form of cell-matrix adhesions. *J. Cell Sci.*, **120**, 137-148.
- [5] Galbraith, C.; Yamada, K. and Sheetz, M. (2002) The relationship between force and focal complex development. *J. Cell Biol.*, **159**, 695-705.
- [6] Evans, E. A. and Calderwood, D. (2007) Forces and bond dynamics in cell adhesion. *Science*, **316**(5828), 1148-1153.
- [7] Zaidel-Bar, R.; Ballestrem, C.; Kam, Z. and Geiger, B. (2003) Early molecular events in the assembly of matrix adhesions at the leading edge of migrating cells. *J. Cell Sci.*, **116**, 4605-4613.
- [8] Hynes, R. (2003) Changing partners. *Science*, **300**, 755-756.
- [9] Cohen, M.; Joester, D.; Geiger, B. and Addadi, L. (2004) Spatial and temporal sequence of events in cell adhesion: from molecular recognition to focal adhesion assembly. *ChemBiochem*, **5**, 1393-1399.
- [10] Erlandsen, S.; Greet Bittermann, A.; White, J.; Leith, A. and Marko, M. (2001) High-resolution CryoFE- SEM of individual cell adhesion molecules (CAMs) in the glycocalyx of human platelets: detection of P-selectin (CD62P), GPI-IX complex (CD42a/CD42balphabeta), and integrin GPIIb/IIIa (CD41/CD61) by immunogold labeling and stereo imaging. *J. Histochem. Cytochem.*, **49**, 809-20.
- [11] Sackmann, E. and Bruinsma, R. F. (2002) Cell adhesion as wetting transition? *Chem. Phys. Chem.*, **3**, 262-269.
- [12] Nicolas, A.; Geiger, B. and Safran, S. A. (2004) Cell mechanosensitivity controls the anisotropy of focal adhesions. *Proc. Natl. Acad. Sci. USA*, **101**, 12520-12525.
- [13] Satyajit, K.; Hanson, D. A. and Schlaepfer, D. D. (2005) Focal adhesion kinase: in command and control of cell motility. *Nat. Rev. Mol. Cell Biol.*, **6**, 56-68.
- [14] Beningo, K.; Dembo, M.; Kaverina, I.; Small, J. and Wang, Y. (2001) Nascent focal adhesions are responsible for the generation of strong propulsive forces in migrating fibroblasts. *J. Cell Biol.*, **153**, 881-888.
- [15] Chen, W. and Singer, S. J. (1982) Immunoelectron microscopic studies of the sites of cell-substratum and cell-cell contacts in cultured fibroblasts. *J. Cell Biol.*, **95**, 205-222.
- [16] Howard, J. (2001) *Mechanics of Motor Proteins and the Cytoskeleton*. Sinauer Associates, Sunderland, Massachusetts.
- [17] Prass, M.; Jacobson, K.; Mogilner, A. and Radmacher, M. (2006) Direct measurement of the lamellipodial protrusive force in a migrating cell. *J. Cell Biol.*, **174**, 767-772.
- [18] Atligan, E.; Wirtz, D. and Sun, S. X. (2006) Morphology of the lamellipodium and the organization of actin associated proteins at the leading edge of crawling cells. *Biophys. J.*, **89**, 3589-602.
- [19] Ballestrem, C.; Hinz, B.; Imhof, B. A. and Wehrle-Haller, B. (2001) Marching at the front and dragging behind: differential $\alpha V\beta 3$ -integrin turnover regulates focal adhesion behaviour. *J. Cell Biol.*, **155**, 1319-1332.
- [20] Galbraith, C. G.; Yamada, K. M. and Galbraith, J. A. (2007) Polymerizing actin fibers position integrins primed to probe for adhesion sites. *Science*, **315**, 992-995.
- [21] Curtis, A. S. (1964) The mechanism of adhesion of cells to glass. A study by interference reflection microscopy. *J. Cell Biol.*, **20**, 199-215.
- [22] Weber, I. (2003). Reflection Interference Contrast Microscopy. *Methods Enzymol.*, **361**, 34-47.
- [23] Creath, K. (1988) *Phase-measurement interferometry techniques in Progress in Optics*. (Wolf, E. Ed.), Elsevier, Amsterdam, Vol. **26**, pp. 349-393.
- [24] Ovryn, B. and Andrews, J. (1998) Phase-shifted laser feedback interferometry. *Opt. Lett.*, **23**, 1078-080.
- [25] Ovryn, B. and Andrews, J. (1999) Measurement of changes in optical path length with nm precision using a phase shifted laser feedback interferometer. *Appl. Opt.*, **38**, 1959-1967.
- [26] Pirouz, K.; Ovryn, B. and McKinley, G. (2004) Microscopic and macroscopic structure of the precursor layer in spreading viscous drops. *Phys. Rev. Lett.*, **91**, 196104-196110.
- [27] Fischer, D. and Ovryn, B. (2000) Interfacial shape and contact-angle measurement of transparent samples with confocal interference microscopy. *Opt. Lett.*, **25**, 478-480.
- [28] Bambino, M. and Ovryn, B. (2006) *Measuring the surface topography at focal adhesions using laser feedback interferometry, in three-dimensional and multidimensional microscopy: image acquisition and processing XIII*, (Conchello, J.-A.; Cogswell, C. J. Wilson, T.; Eds.), Proc. of SPIE. Vol. **6090**, pp. 60900F-1 -60900F-7.
- [29] Wang, W.; Wyckoff, J. B.; Frohlich, V. C.; Oleynikov, Y.; Huttelmaier, S.; Zavadil, J.; Cermak, L.; Bottinger, E. P.; Singer, R. H.; White, J. G.; Segall, J. E. and Condeelis, J. S. (2002) Single cell behavior in metastatic primary mammary tumors correlated with gene expression patterns revealed by molecular profiling. *Cancer Res.*, **62**, 6278- 6288.